3D Facial Similarity Measurement and Its Application in Facial Organization

CHENLEI LV, ZHONGKE WU, XINGCE WANG, and MINGQUAN ZHOU,
School of Artificial Intelligence, Beijing Normal University, China

We propose a novel framework for 3D facial similarity measurement and its application in facial organization. The construction of the framework is based on Kendall shape space theory. Kendall shape space is a quotient space that is constructed by shape features. In Kendall shape space, the shape features can be measured and is robust to similarity transformations. In our framework, a 3D face is represented by the facial feature landmarks model (FFLM), which can be regarded as the facial shape features. We utilize the geodesic in Kendall shape space to represent the FFLM similarity measurement, which can be regarded as the 3D facial similarity measurement. The FFLM similarity measurement is robust to facial expressions, head poses, and partial facial data. In our experiments, we compute the distance between different FFLMs in two public facial databases: FRGC2.0 and BosphorusDB. On average, we achieve a rank-one facial recognition rate of 98%. Based on the similarity results, we propose a method to construct the facial organization. The facial organization is a hierarchical structure that is achieved from the facial clustering by FFLM similarity measurement. Based on the facial organization, the performance of face searching in a large facial database can be improved obviously (about 400% improvement in experiments).

CCS Concepts: • **Computing methodologies** → **Shape representations**; **Shape analysis**;

Additional Key Words and Phrases: Kendall shape space, facial feature landmarks model, face recognition, facial data organization

ACM Reference format:
Chenlei Lv, Zhongke Wu, Xingce Wang, and Mingquan Zhou. 2020. 3D Facial Similarity Measurement and Its Application in Facial Organization. *ACM Trans. Multimedia Comput. Commun. Appl.* 16, 3, Article 82 (July 2020), 20 pages.
https://doi.org/10.1145/3397765

1 INTRODUCTION

Biometric information has become extremely useful in modern life. As a popular type of biometric information, the human face has been researched for many years and successfully applied in multimedia fields such as digital security, network communication, film production industry, and so on. As one of the most fundamental tasks in facial analysis, facial similarity measures frameworks [5, 10] can be used to represent the "distances" between different faces for quantitative facial analysis, which has attracted considerable attention from researchers. In the 2D scenes, the computation of

Authors' addresses: C. Lv, Z. Wu, X. Wang, and M. Zhou, School of Artificial Intelligence, Beijing Normal University, Beijing, China; emails: chenleilv@mail.bnu.edu.cn, {zwu, wangxingce, mqzhou}@bnu.edu.cn.

1551-6857/2020/07-ART82 $15.00
https://doi.org/10.1145/3397765

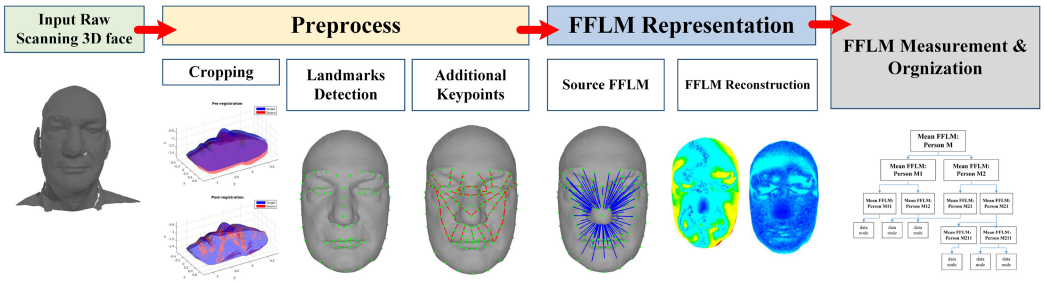

Fig. 1. The pipeline of our framework.

facial similarity [50, 54] is affected by various conditions, such as head poses, facial expressions, natural noise, cosmetics, and illumination. Since 3D scanning devices and related technology have been widely utilized in capturing 3D objects, using 3D scanning facial data in facial similarity measures research has become possible. Based on the global geometric features in the 3D face, the facial similarity measures are robust to texture information, such as lighting and cosmetics.

Although there are many advantages of constructing facial similarity measurement based on 3D faces, some influencing factors that affect the accuracy of the measurement (expressions, rough triangulated meshes, and occlusion regions) should be considered carefully. To solve the problem, we propose a facial similarity measurement and organization framework based on Kendall shape space theory [36]. The framework is mainly composed of four components: (1) pre-processing for face registration [3], facial landmarks, and additional keypoints extraction; (2) FFLM construction from source 3D face; (3) FFLM reconstruction to remove the influence of facial expressions; and (4) similarity measurement of different FFLMs via geodesic distance computation in Kendall shape space. Besides, we also explore the application of the proposed 3D facial similarity measurement on facial organization. The construction of facial organization involves clustering FFLMs into different subclasses based on their similarity and then building a tree structure for faces storing. The FFLMs with similar shape information are placed into the same subclass. We present the pipeline of our framework in Figure 1. For face recognition in a large database, the matching performance can be improved considerably based on the facial organization.

In summary, our main contributions are as follows:

(1) We propose a novel facial similarity measurement method based on Kendall shape space theory. Traditional applications based on Kendall theory focus on medical image processing and simple 3D object shape analysis [19, 24]. We utilize the metric tools from Kendall theory to build facial similarity measurement, which is more robust and accurate.
(2) We propose the FFLM for 3D face representation. The FFLM can be regarded as a reconstruction form of a 3D face. The influence of facial expression can be removed from the FFLM by using an optimization method in Kendall shape space, while the identity features are preserved.
(3) We propose a facial organization method based on facial similarity measurement. The organization can be used to improve the speed of face matching in a large facial database.

The rest of the article is organized as follows: In Section 2, we discuss the related works on 3D facial similarity measures. The basic theory of Kendall shape space is presented in Section 3. In Section 4, the pre-processing of 3D scanning facial data is discussed. In Sections 5 and 6, we illustrate the FFLM construction method and facial similarity measures in Kendall shape space. The construction of facial organization based on the facial similarity measures is introduced in

Section 7. In Section 8, we present experiments on public facial databases to evaluate the performance of the facial similarity measurement and facial organization in our framework.

2 RELATED WORKS

Generally, 3D facial similarity measures methods extract geometric features from 3D face to build measurement, which is divided into three categories according to the different types of geometric features: modeling-based, global region-based, and local region-based.

Modeling-based methods construct the framework of the facial measures based on the reconstructed facial model. The reconstruction process establishes a regular facial model for different faces and retains robust geometric features that could support accurate facial measures. The 3D Morphable Model is a classical facial modeling method and has been widely used in 3D facial measures [8, 9, 22, 26, 37]. There are also many studies that use bilinear model to reconstruct faces for recognition purpose [15, 47, 48]. Li [41] proposed a facial expression analysis method that was based on multi-features analysis. Xu [45] developed a data-driven face detection method based on the Gaussian mixture model. Bronstein [10] proposed a canonical form for 3D face recognition. Ansari [4] proposed a pipeline for 3D modeling and recognition of facial images from two orthogonal views. Zeng [63] proposed a facial representation using Ricci flow in the face-matching process. Recently, using the Riemannian geometric framework to construct the face model in face recognition is popular. Patel [49] used manifold optimization instead of linear operation in a face modeling framework. Kurtek [38] proposed a statistical framework for facial modeling in surface shape space. Drira [17] proposed a facial shape analysis framework for 3D face recognition.

Global region-based methods extract facial features from 3D face to achieve facial measurement directly. Some methods defined the distance between two 3D faces in R^3 space, such as points' distance based [29, 60] and curves based [20, 32, 33, 39]. Some works attempted to combine the machine learning framework and the facial features from R^3 space to improve the recognition rate. Ahdid [2] combined iso-geodesic curves and space reduction methods (principal component analysis and Fisher linear discriminant analysis) to construct an automatic 3D face recognition system. They improved the framework using Jacobi iterations to solve the Eikonal equation [1]. Other methods constructed 3D face-matching frameworks based on global facial features directly. Berretti [5] proposed a method that used iso-geodesic stripes and 3D weighted walkthroughs to achieve face-matching results. Tang [59] proposed a principal curvature measure estimation for 3D face recognition. Lv [44] constructed the facial measurement in parameter domain.

Local region-based methods extract local shape descriptors from different facial regions to construct facial matching framework. Some methods attempted to construct local shape descriptors based on keypoints in 3D face [6, 7, 27, 40]. The others constructed local shape descriptors from facial surface [25, 30, 31, 35, 39, 55, 56]. Some methods constructed the face recognition framework based on partial facial region. The partial facial region can be selected from the nasal region or ear region. In terms of the nasal region, Drira [18] proposed a nasal shape analysis framework using elastic geodesic circle measures in a Riemannian framework. Mahmood [46] proposed a partial face-matching method that constructed local shape descriptors from the nasal region. Emambakhsh [21] proposed a partial face recognition framework based on different curves in the nasal region. Lv [43] proposed nasal similarity measurement based on nasal curves. In terms of the ear region, Chen [12] proposed an ear recognition method based on local surface patch representation. Yan [61] proposed an ear recognition method using curvature estimation and surface segmentation. Yuan [62] proposed an ear recognition framework based on a nonnegative dictionary and sparse representation. Zhang [64] proposed a 3D ear recognition method based on sparse coding and a multi-class linear classifier simultaneously.

In summary, modeling-based methods construct the regular facial model from source 3D face. Based on the facial model, some influential factors (facial expressions and head poses) are removed. However, the quality of facial models, such as the 3D morphable model and bilinear model, depends on training facial samples. The modeling process increases the complexity of the algorithm and various types of occlusion affect the accuracy of the modeling results. Global region-based methods extract geometric features from 3D face directly. Such methods depend on the quality of the facial surface. Various influences, such as expressions and occlusions, are difficult to remove. Local region-based methods are robust to facial expressions and missing data in faces. However, such methods cannot achieve global facial measures results. In our framework, we attempt to construct a framework that achieves the advantages of modeling-based methods and local region-based methods. The facial similarity measurement in our framework is robust to facial expressions, head poses, and different occlusions. Before introducing our method, we present the fundamentals of Kendall shape space theory.

3 KENDALL SHAPE SPACE THEORY

Kendall shape space [36] can be regarded as a quotient space, which is used to measure the similarity between different "shapes" in geometric view. The discrete form of a "shape" in Kendall shape space is represented by points sequences, which is robust to similarity transformations (scaling, translation, and rotation). In this subsection, we introduce some background knowledge and mathematical tools of Kendall shape space theory.

3.1 Kendall Shape Space

The Riemannian manifold [36] is constructed by "shapes," or points sequences, specifically. To be a quotient space, Kendall shape space removes the influence of similarity transformation from the Riemannian manifold. The construction of the Kendall shape space can be considered as a remapping from the Riemannian manifold. The "shapes" in a similarity transformation group of the manifold are remapped to single reflection in Kendall shape space. Therefore, the influences of similarity transformation are removed from the Riemannian manifold to Kendall shape space. To construct a Kendall shape space, the Riemannian manifold should be defined at first. Let $X = (x_1, \ldots, x_k)$, which is a points sequence and used to represent the discrete form of shape. In Equation (1), the Riemannian manifold is defined by X.

$$M = R^{m \times k} \backslash \{0\}, X \in M \tag{1}$$

M represents the Riemannian manifold constructed by points sequences, $X \in M$. The m is the dimension number of one point in X. Based on X, it can be known that M is an $m * k$-dimensional differential manifold.

Following the definition, the Kendall shape space $[D]$ is achieved from M, which removes the similarity transformation G in Equation (2). The a and b are two elements in M with same form to X. $D(a)$ and $D(b)$ are two reflections of a and b in $[D]$. In $[D]$, the geodesic distance $d_{Kendall}$ between $D(a)$ and $D(b)$ is invariant in G. The $d_{Kendall}$ is the key value to measure the similarity between different shapes (a and b). Generally, the computation of $d_{Kendall}$ in [D] is complex, because the construction of [D] is difficult. However, in Reference [36], it has been proved that the $d_{Kendall}$ can be achieved from the M directly using Equation (3). The property research of $[D]$ can be transferred in M. In Section 3.2, we introduce an analysis tool (Procrustes analysis) for $d_{Kendall}$ computation.

$$M/G = \{[D] | D \in M\} \tag{2}$$

$$d_{Kendall}\left(D(a), D(b)\right) = \inf_{g \in G} d_M\left(D(a), g.D(b)\right) \tag{3}$$

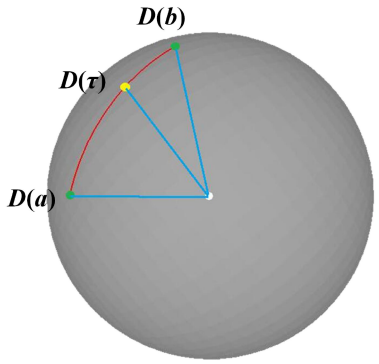

Fig. 2. The geodesic path between $D(a)$ and $D(b)$ in Kendall shape space. $D(\tau)$ is the shape unit in the path.

3.2 Procrustes Analysis

To solve the Equation (3), the influence of G should be removed, which can reduce the difficulty of optimization. To remove the influence of similarity transformation G, centroid alignment and scaling normalization are performed. We illustrate this process in Equation (4) and Equation (5).

$$\begin{aligned} D_s(a) &= (x_{(1)} - \bar{x}, \ldots, x_{(k)} - \bar{x})/s(a) \\ \bar{x} = \frac{1}{k}\sum_{j=1}^{k} x_{(j)}, s(a) &= \left(\sum_{j=1}^{k} \left\| x_{(j)} - \bar{x} \right\|\right)^{1/2} \end{aligned} \tag{4}$$

$$d_{Kendall}\left(D(a), D(b)\right) = \inf_{O \in G} d_{S_m^k}\left(D_s(a), O.D_s(b)\right) \tag{5}$$

$\bar{x}$ is the centroid of a, and $s(a)$ is the scale of a. Taking each point in a minus the centroid and divided by $s(a)$, the new form $D_s(a)$, which has removed the translation and scale factors, is achieved. Based on Equation (4), a new shape measurement is proposed in Equation (5). O represents the rotation group. S_m^k represents the pre-shape space of Kendall shape space, which has removed the scaling and translation factors.

To remove the influence of rotation, the alignment of the points sequence should be computed. The process can be transformed into a singular value decomposition (SVD) problem [36]. The $tr(\Lambda)$ represents the trace of matrix (product of $D_s(a), D_s(b)$), and the $d_{Kendall}$ in the Kendall shape space is achieved in Equation (6), which is called the Procrustes analysis.

$$\begin{aligned} d_{\text{Kendall}}\left(D(a), D(b)\right) &= \inf d_{S_m^k}\left(D_s(a), O.D_s(b)\right) \\ &= arccos\text{tr}(\Lambda) \end{aligned} \tag{6}$$

$$\begin{aligned} D(\tau) &= \frac{1}{\sin(\theta)}(\sin(\theta(1-\tau))D(a) + \sin(\theta\tau)D(b)) \\ \theta &= d(D(a), D(b)), \tau \in [0,1] \end{aligned} \tag{7}$$

The new shape can be constructed by following the geodesic path between two shapes $D(a)$ and $D(b)$. In Equation (7), we present the new shape construction procedure. The θ is the intersection angle between two shapes $D(a)$ and $D(b)$ in the space, which is equal to the geodesic distance. The τ is a parameter that defines the position in the geodesic path between $D(a)$ and $D(b)$. In Figure 2, we illustrate the geodesic path between $D(a)$ and $D(b)$ in Kendall shape space.

4 PRE-PROCESSING

Based on Kendall theory, the task of facial similarity measures can be regarded as the geodesic distance computation in Kendall shape space. Providing the discrete points sequence representation

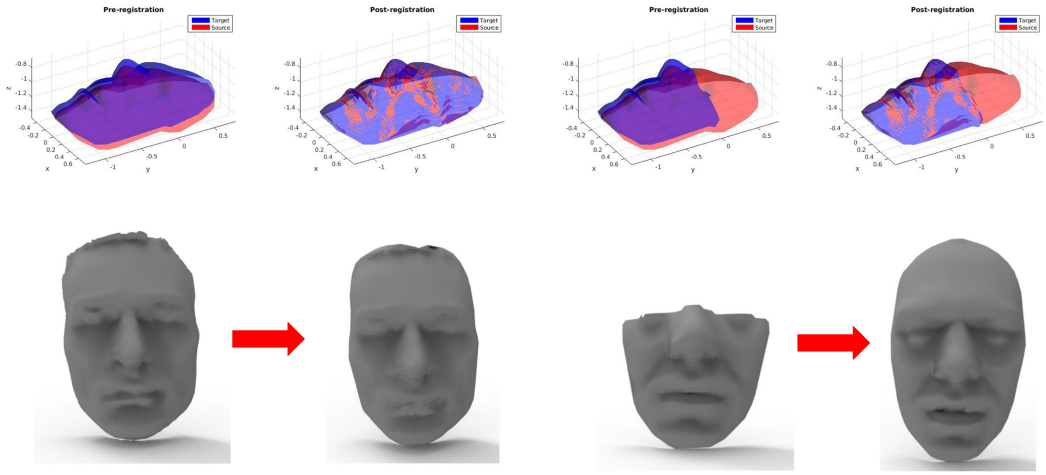

Fig. 3. Face cropping by non-rigid transfer. The top line represents the reconstruction process, from raw scanning faces to template facial surface. The following line shows the registration facial surface result.

of facial shape features, the related tools of Kendall theory can be used directly. In this section, we will discuss the details of the points sequence construction.

4.1 Cropping for Raw Scanning Facial Data

Following the Kendall theory, we should extract the facial shape features first. The facial shape features are represented by facial landmarks in many works, such as the active shape model (ASM) [14] and the active appearance model (AAM) [13]. Generally, facial landmarks detection cannot be used directly in raw 3D scanning face because of the influence of missing data and noise in the local facial region. Therefore, the facial cropping is necessary for a raw 3D face. In our framework, we extract the facial region by Reference [9] and utilize a surface registration method, non-rigid iterative closest point (NICP) [3], to carry out the cropping task. In Figure 3, we present two instances of facial cropping. After the cropping process, the raw 3D scanning face can be aligned and normalized into a regular facial surface, and the partial facial surface can be repaired by the template facial data.

4.2 3D Facial Landmarks Detection

Based on the regular facial surface, a 3D facial landmarks detection method can be used for landmarks detection. The 3D facial landmarks detection methods of References [16, 34, 51, 57] are based on the geometric features of the 3D facial surface. We use the facial landmarks detection method of Reference [57] to achieve a set of coarse facial landmarks. To harvest more accurate facial landmarks, we attempt to match the regular facial model to a 3D morphable model [65] based on coarse facial landmarks. The basic idea is inspired by Reference [28]. The accurate facial landmarks have been labeled in the 3D morphable model. The details of our facial landmarks detection scheme are illustrated in Figure 4.

4.3 Additional Keypoints

The facial landmarks from the facial surface can be used to represent the facial shape features, including the eyes, nose, mouth, and facial contours. However, facial landmarks cannot be used to represent the global facial surface. To represent the global facial surface, some additional

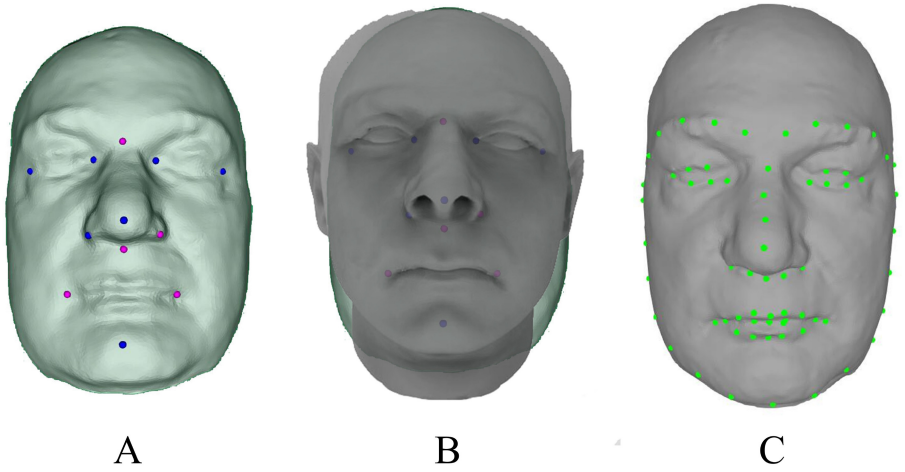

Fig. 4. 3D facial landmark detection scheme in our framework. A: The coarse facial landmark result; B: 3D morphable model matching results; C: Final facial landmarks results (68 points).

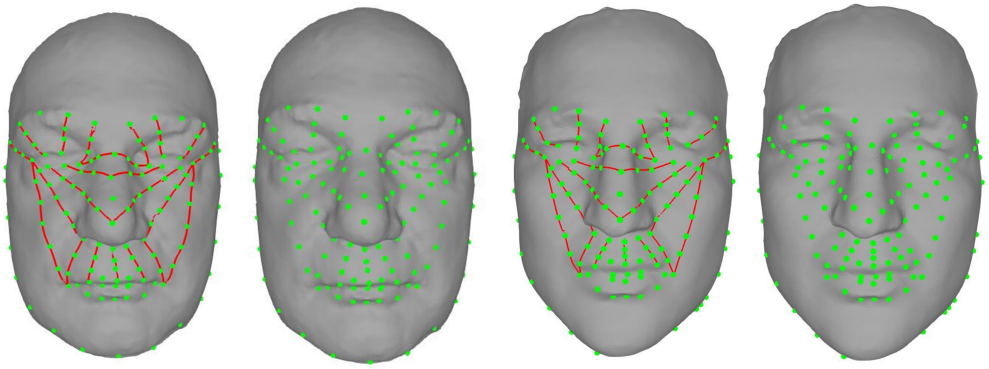

Fig. 5. Instances of facial landmarks and additional keypoints. The red curves are the geodesic paths between facial landmarks.

keypoints on the facial surface must be searched to cover the entire facial region. In our framework, we compute the geodesic paths [58] between different facial landmarks in the facial surface. The additional keypoints are labeled in the geodesic paths according to fixed step length. The advantage of geodesic path–based keypoints detection is that the different keypoints are approximately equidistant for various facial expressions [10]. We connect the facial landmarks from different facial regions to construct a keypoints net, which can be used to represent a discrete form of the facial surface. The details of additional keypoints' extraction are discussed in experiments. In Figure 5, we present some instances of facial surfaces with facial landmarks and additional keypoints. After the detection process, we obtain enough facial landmarks and additional keypoints for FFLM construction.

5 FACIAL FEATURE LANDMARKS MODEL

Based on the facial landmarks and additional keypoints in a 3D face, we propose a facial feature landmarks model (FFLM) to represent facial shape features. Following the Kendall theory, the

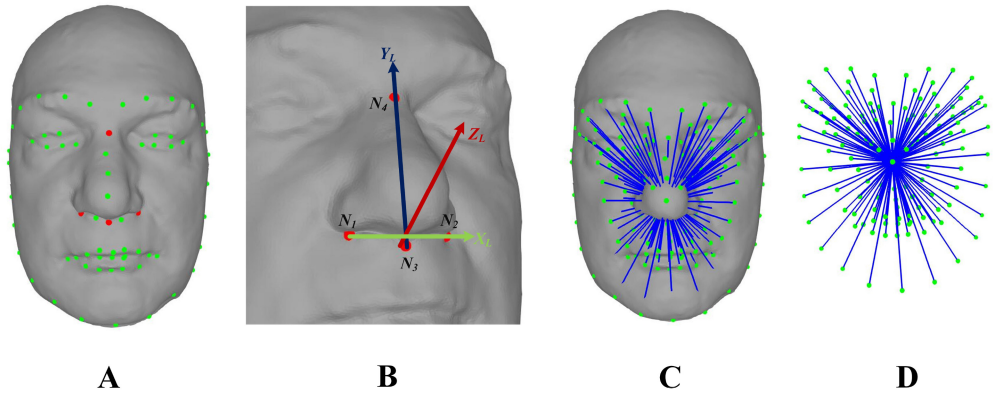

Fig. 6. Instance of the local coordinate system and the FFLM. A: The red points represent the facial landmarks selected from the nasal region to construct the local coordinate system; B: N_1 to N_4 are used to construct the local coordinate system (First, we connect N_3 to N_4 to represent the Y_L axis. Second, we connect N_1 to N_2 and compute the Z_L axis from $N_3N_4 \times N_1N_2$. Finally, we obtain X_L from $Y_L \times Z_L$.); C: The discrete form of the FFLM in the 3D face; D: The pure discrete form of the FFLM.

influence of similarity transformations should be removed from the FFLM. In the following part, we introduce the construction of the FFLM and the similarity transformation removal method.

We align the center of the points sequence of FFLM first. In our framework, the center of the points sequence is not the average center, but the nasal tip in a 3D face. The reason is the influence of facial expression is not removed, which affects the relative positions of the points. The nasal tip's position is limited by the skull, which is more stable. In Equation (8), we align the points sequence based on the nasal tip, which removes the influence of translation.

$$\begin{aligned} D_F &= \{x_1, \ldots, x_k, x_N\}, \\ Lv_t &= \{v_1, \ldots v_k\}, v_i = x_i - x_N \end{aligned} \tag{8}$$

D_F is the points sequence from the 3D face that includes facial landmarks and additional keypoints. X_N is the nasal tip from the D_F. Lv_t is the points sequence, which is aligned by X_N. Next, the influence of scaling should be removed. We compute the scale of Lv_t and use it to normalize Lv_t. In Equation (9), Lv_{ts} is obtained, which removes the scale $s(Lv_t)$ from Lv_t.

$$\begin{aligned} s(Lv_t) &= \left(\sum_{i=1}^{k} \|v_i\| \right), v_i \in Lv_t \\ Lv_{ts} &= \{v'_1, \ldots v'_k\}, v'_i = \frac{v_i}{s\,(Lv_t)}, \sum_{i=1}^{k} \|v'_i\| = 1 \end{aligned} \tag{9}$$

Equation (8) and Equation (9) are consistent with Equation (4), and the influences of translation and scaling are removed from the new points sequence Lv_{ts}. In our framework, the influence of rotation can be removed by the facial landmark alignment process. We select several facial landmarks from the nasal region, which are robust to the facial expressions, to align the local coordinate system. In Equation (10), we achieve the final representation of the facial shape features, which can be regarded as the FFLM of the facial data. The coordinate transformation function T is used to transfer points in Lv_{ts} into the local coordinate system, which is constructed by facial landmarks from the nasal region. In Figure 6, we illustrate the local coordinate system and the instance of FFLM.

$$Lv_{tsr} = \{T(v'_1), \ldots, T(v'_k)\} \tag{10}$$

6 FACIAL SIMILARITY MEASUREMENT

We propose the facial similarity measurement based on the FFLM. Theoretically, the geodesic distance of different FFLMs is computed in Equation (11), and $Lv_{tsr}(a)$ and $Lv_{tsr}(b)$ represent two FFLMs.

$$d_{\text{Kendall}}\left(Lv_{tsr}(a), Lv_{tsr}(b)\right) = arccos(Lv_{tsr}(a) \cdot Lv_{tsr}(b)) \tag{11}$$

However, the influence of facial expressions is not removed from the FFLM. To address this issue, we propose an FFLM reconstruction method based on a geodesic path search in Kendall shape space (GPSK [42]). Using GPSK, the facial attributes of the source FFLM can be decoupled: expression and identity, which are controlled by parameters of GPSK.

6.1 Reconstructing FFLM

The reconstruction of the source FFLM includes three steps: (1) Achieving template FFLM database from a template facial database that has regular labels of facial expressions and identities; (2) Searching for the initial FFLM from the template FFLM database that has the minimum geodesic distance to the source FFLM; (3) Optimizing the initial FFLM to obtain the final reconstructed FFLM using a geodesic path search in Kendall shape space (GPSK). The template FFLM database can be achieved by Equation (8) to Equation (10). In Equation (12), we show the function for initializing an FFLM from the template FFLM database. F_t represents the template facial database, F_i represents the face in F_t, and F_s represents the source face. The initial FFLM $Lv_{tsr}(F_{init})$ is the FFLM of F_i that has the minimum geodesic distance to $Lv_{tsr}(F_s)$ in Kendall shape space.

$$\begin{aligned} Lv_{tsr}(F_{init}) = \{Lv_{tsr}(F_i) | \min d_{Kendall}(Lv_{tsr}(F_i), Lv_{tsr}(F_s)), \\ F_i \in Ft\} \end{aligned} \tag{12}$$

The initial FFLM $Lv_{tsr}(init)$ can be regarded as the starting point for GPSK. The GPSK in our framework involves searching the direction of the geodesic path iteratively based on the FFLMs from Ft and generating the new FFLM in Kendall shape space in Equation (7). The GPSK for FFLM construction is decoupled from the facial attributes (identity and expression) in our framework. The target of GPSK is to reduce the geodesic distance between the reconstructed FFLM and source FFLM. The distance is represented by two facial attribute optimizations in Equation (13).

$$\begin{aligned} E_{expression} = d_{Kendall}(Lv_{tsr}(F_i), Lv_{tsr}(F_s)), \\ F_i \in F_{expression} \\ E_{identity} = d_{Kendall}(Lv_{tsr}(F_i), Lv_{tsr}(F_s)), \\ F_i \in F_{identity} \end{aligned} \tag{13}$$

In detail, the basic computation of GPSK in each iteration includes two steps: (1) searching the expression candidate FFLMs in Ft that have the same identity label as the initial FFLM and generating new FFLM with new expression; (2) searching the identity candidate FFLMs in Ft that have the same expression label as the initial FFLM and generating new FFLM with new identity. For step 1, the expression candidate set is represented by $F_{expression}$ in Equation (13). Similarly, the identity candidate set is represented by $F_{identity}$. We propose the new FFLM generation method in Equation (14), which is derived from Equation (7) and used to generate the new FFLM $Lv_{tsr}(F_{new})$ in Kendall shape space.

$$\begin{aligned} Lv_{tsr}(F_{new}) = \frac{1}{\sin(\theta)}(\sin(\theta(1-\tau))Lv_{tsr}(F_{init}) \\ + \sin(\theta\tau)Lv_{tsr}(F_i)) \\ \theta = d(Lv_{tsr}(F_{init}), Lv_{tsr}(F_i)), \tau \in [0,1] \end{aligned} \tag{14}$$

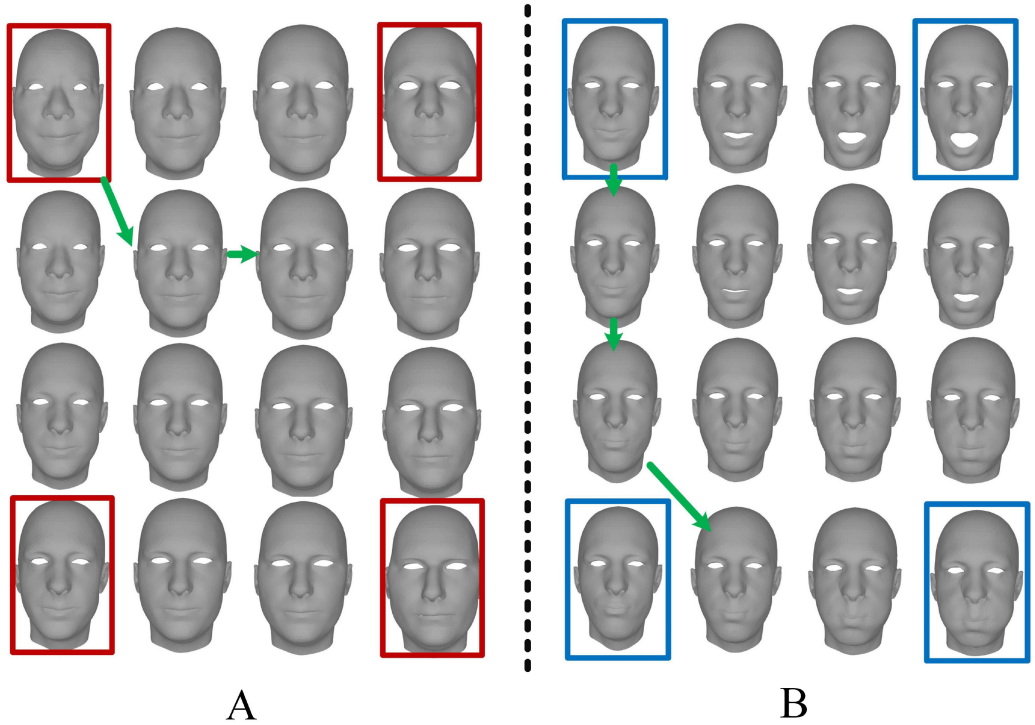

Fig. 7. Instance of the GPSK for expression and identity optimization. In part A, the facial data with a red frame are template faces with different identities and the same expression from the database. In part B, the facial data with a blue frame are template faces with different expressions and the same identity from the database. The green arrows represent the geodesic path searching directions. The new faces are generated by following the arrows.

The GPSK can be compared to the linear optimization process. The new FFLMs are synthesized by existing FFLMs. The difference is the GPSK generates new FFLMs in Kendall shape space, which is not a linear space. The optimization results are more consistent with the natural facial expressions transfer and facial identity shape features. Using the GPSK, the initial FFLM is updated constantly until $E_{expression}$ and $E_{identity}$ are not decreasing. The iteration is stopped when the energy values in Equation (13) are below a threshold, and the reconstructed FFLM is achieved. After this process, the new FFLM with the new expression and identity label is generated. In Figure 7, we present an example to explain the process of GPSK.

6.2 Facial Similarity Measurement for FFLMs

We propose the facial similarity measurement based on the reconstructed FFLM. We select the FFLM that has the same identity label as the reconstructed FFLM and the natural expression label, then the reconstructed FFLM is transferred to the regular FFLM (without expression). In Equation (15), we show the expression removal function for the source FFLM.

$$\begin{aligned} M_{transfer} &= Lv_{tsr}(F_{regular}) - Lv_{tsr}(F_{reconstruction}) \\ Lv_{tsr}(F_{final}) &= Lv_{tsr}(F_s) + M_{transfer} \end{aligned} \tag{15}$$

$M_{transfer}$ represents the expression transfer from the reconstructed FFLM $Lv_{tsr}(F_{reconstruct})$ to the regular FFLM $Lv_{tsr}(F_{regular})$. The final FFLM $Lv_{tsr}(F_{final})$ can be obtained by using the

$M_{transfer}$ to transfer the source FFLM $Lv_{tsr}(F_s)$, which removes the influence of facial expressions from source face. The operation can be viewed as an approximation; that is, the transfer between reconstructed FFLM and regular FFLM approximates the source FFLM to final FFLM. Based on the final FFLM, the expression-robust facial similarity measurement can be obtained from Equation (11).

Based on the similarity measurement, an effective facial organization is constructed. In the following section, we will discuss the facial organization.

7 FACIAL ORGANIZATION

We propose a facial organization based on our facial similarity measurement. Generally, the face-searching process in a large facial database incurs a high computational cost. In our framework, we divide the faces into subclasses based on the facial similarity measurement. The subclasses can be organized into a hierarchical structure. The face-searching process in a large facial database can be divided into subtasks in this structure. Here, we explain the details of the facial organization.

We define the mean FFLM as the data center of a subclass. The mean FFLM represents the global shape features of a subclass. In Equation (16) and Equation (17), we present the computation of the mean FFLM.

$$S = \{F_1, \ldots F_n\},$$
$$V(Lv_{tsr}(F_m)) = \sum_{i=1}^{n} d(Lv_{tsr}(F_m), Lv_{tsr}(F_i)) \tag{16}$$

$$\overline{Lv_{tsr}(F)} = \arg\min_{F_m \in S} V(F_m) \tag{17}$$

S is the subclass of FFLMs in the facial dataset, and V is the sum of the distances from an FFLM to other FFLMs in set S. The mean FFLM $\overline{Lv_{tsr}(F)}$ of S is the FFLM that has the minimum value of V in set S. The facial clustering method is used to find different mean FFLMs of different subclasses in a large facial database. We use the AP clustering method [23] to obtain the mean FFLMs and subclasses. The similarity measurement values of different FFLMs from the facial database are taken as an input matrix for AP clustering. After the clustering process, the 3D faces from the database can be divided into different subclasses with similar mean FFLM (clustering center). When the amount of 3D faces in a subclass is larger than a specified threshold, we iteratively implement the AP clustering until the number of 3D faces in each subclass is less than the threshold. Finally, a hierarchical structure can be constructed based on the subclasses in different levels.

In Figure 8, we illustrate the process of constructing the hierarchical structure. Faces $F1$ to Fn from different persons in the facial database are used to construct the FFLMs. The distance matrix (d_{11} to d_{nn}) of different persons is constructed by the similarity measurement. M represents the person with the mean FFLM from the whole facial database. $M1$ and $M2$ represent the person with the mean FFLM in the second-level subclasses. Based on the facial organization structure, the scale of the face-searching task in a large database is obviously reduced. In experiments, we show the improvement of face searching based on the organization.

8 EXPERIMENTS

We evaluate the performance of the facial similarity measurement and facial organization. The hardware platform is constructed by Intel Xeon E5620 2.4 GHz, 12 G RAM, and TITAN XP. The facial expression database, Facewarehouse [11] (150 persons × 20 expressions), is used to be the template facial database and reconstruct the FFLM. The other two facial databases, FRGC2.0 [52] and BosphorusDB [53], are used to evaluate the accuracy of the similarity measurement. We construct the different test sets from the two facial databases and compare different methods on

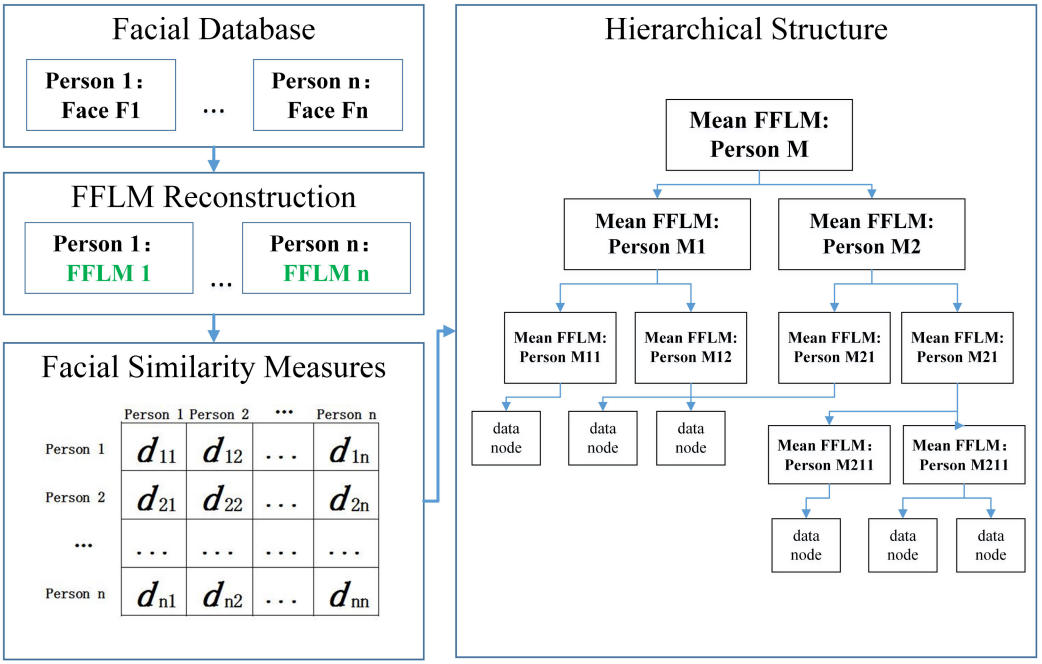

Fig. 8. Construction of the hierarchical structure based on the distances between the reconstructed FFLMs.

face recognition tasks. Based on the similarity measurement, we construct the facial organization and evaluate the performance. The improvement of face-searching speed based on the facial organization is evaluated.

The additional keypoints should be defined clearly. The additonal keypoints extraction should follow two rules: (1) the geodesic path for keypoints location should not cross the regions that include the eyes and mouth; (2) the sampling density of keypoints should be proportional to the size of the face area. The eye and mouth regions contain complex geometric information that influences the accuracy of the keypoints' positions. Following these two rules, we propose a configuration to guide the additional keypoints extraction. In Figure 9, we present the additional facial keypoints extraction configuration. $M_{transfer}$ is used to remove the influence of expression from a 3D face when the FFLM includes all vertices. In Equation (15), $M_{transfer}$ is used to remove the influence of facial expression. Once the FFLM is extended to the global facial surface, $M_{transfer}$ can be used to represent the facial surface transfer between different expressions. Through face alignment and the neighbor point interpolation algorithm, the expression removal process can be achieved for a 3D face. In Figure 10, we show the expression removal instances.

8.1 Robustness for Different Facial Expressions

To show the performance of the FFLM reconstruction, we propose the experiments for facial expressions robustness evaluation. We use a 10-fold cross-validation test in FRGC2.0 and BosphorusDB. A subclass of probe set includes 285×2 samples in FRGC2.0 and 105 samples in BosphorusDB (the sets do not include different types of occlusions and head poses). In Figures 11 and 12, we show the receiver operating characteristic curves (ROC) and cumulative matching characteristics (CMC) results to illustrate the improvement in accuracy for the FFLM reconstruction. The results from "Without reconstruction" are achieved from the FFLM without reconstruction, which

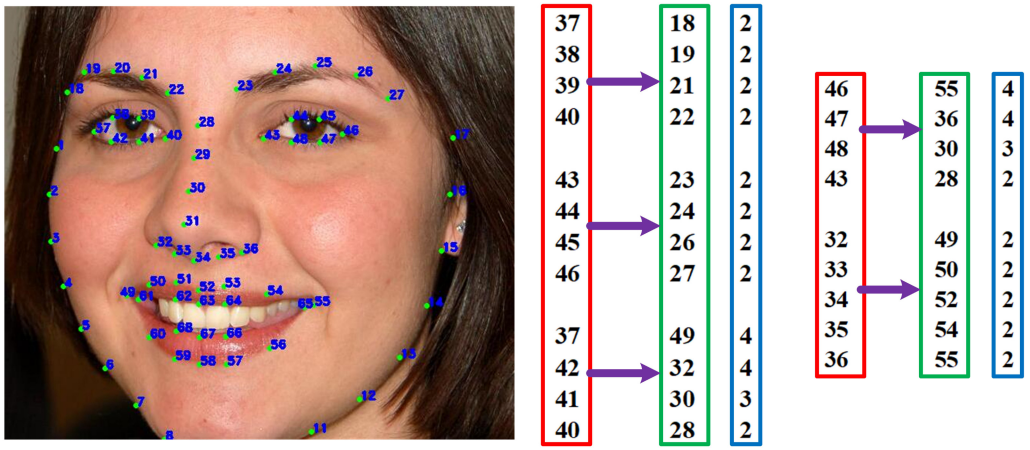

Fig. 9. The additional keypoints extraction configuration. In the left picture, the facial landmarks labels (blue number) show the basic information used to locate the different facial landmarks. In the right picture, we use a purple box to represent the geodesic path between related facial landmarks (red represents the start, green represents the end) and sign the sampling rate for the additional keypoints labels.

means the expression influences are not removed from the measurement. The results from "Reconstruction1" mean the FFLM is constructed by facial landmarks without additional keypoints, which means the FFLM is not a global facial shape representation. The results from "Reconstruction2" mean the FFLM with reconstruction and all points. The comparison of the results shows that the reconstruction and additional keypoints improve the accuracy of the measurement obviously.

Based on the different test sets, we evaluate the identification accuracy of different facial measures methods. Even for those methods [17, 18] that construct a face-matching framework based on shape space, which is similar to our method, the matching accuracy is affected by the quality of the facial surface. The elastic shape measure for certain curves is not strictly a facial expression robustness algorithm. Berretti [5] proposes a facial measures method based on geodesic stripes that are robust to different facial expressions. However, the method is sensitive to head poses, which affects the accuracy of the facial similarity measurement. Some researchers [7, 40] propose 3D face recognition methods based on keypoints features that achieve high accuracy for 3D faces with partial surfaces and do not require high-quality meshes. However, the performance of the method depends on the density of keypoints in the facial data, which does not support accurate quantitative facial analysis.

In Table 1, we evaluate the identification and verification rate of different methods in two facial test sets in terms of FAR0.1 and Rank1. We collect the results of other methods from original published data and code reproduction (for Drira and Berriti). For further evaluation of the influence of expressions on face recognition, we construct subsets from BosphorusDB (105×15 samples totally and 105×8 with expressions). In Table 2, based on the subsets, we evaluate the identification rate in Rank1 of different methods.

8.2 Robustness for Different Occlusions

BosphorusDB contains various types of occlusions and poses in the 3D faces. We select 105*5 samples from 105 persons to build the probe set. In most cases, the keypoints are extracted from the nasal region under various types of occlusion. To facilitate the keypoints extraction, we limit the effective region to the nasal area. For some facial data affected by extreme poses and occlusions, we have only one-half of the facial surface; we extract the keypoints from the effective part to build

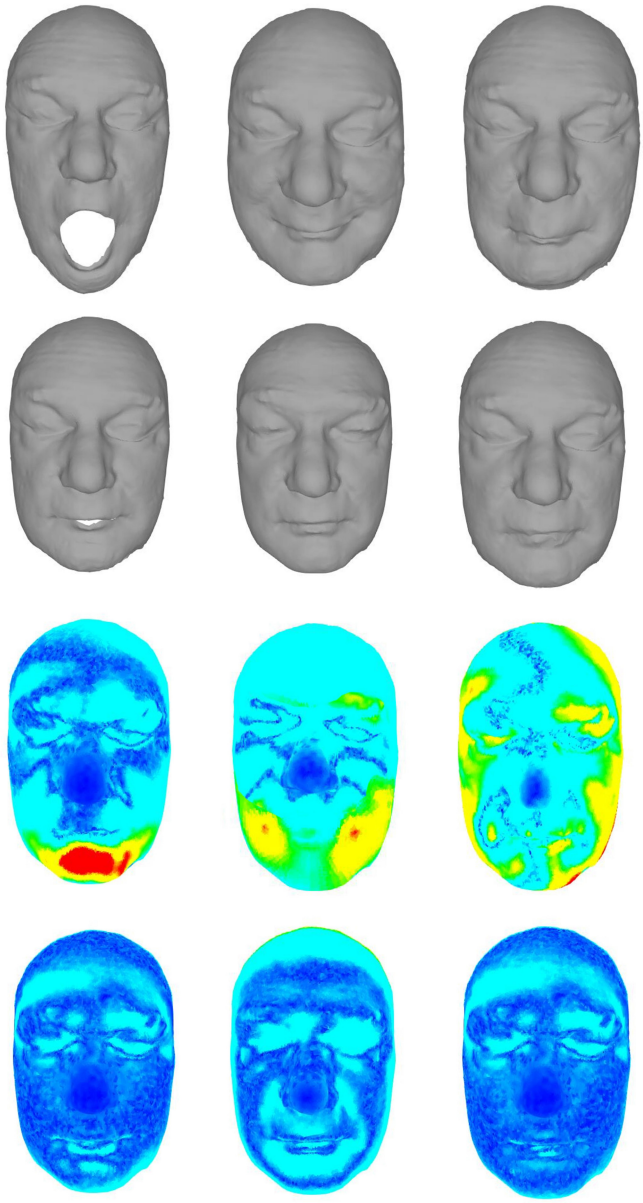

Fig. 10. Examples of the expression removal process. The first row represents the 3D faces with different expressions. The second row represents the 3D faces after the expression removal process. The bottom two rows represent the root-mean-square (RMS) errors for the top two rows (different faces to a regular face with a neutral expression. The distance value is limited between 0 mm and 1.2 mm).

the local final FFLM. We select different types of data from BosphorusDB to construct subsets. In Figure 13, we show the ROC and CMC results of our method in different subsets.

The global features–based method cannot achieve effective facial analysis results based on 3D faces with different kinds of occlusions. Some methods that are based on local features or nasal

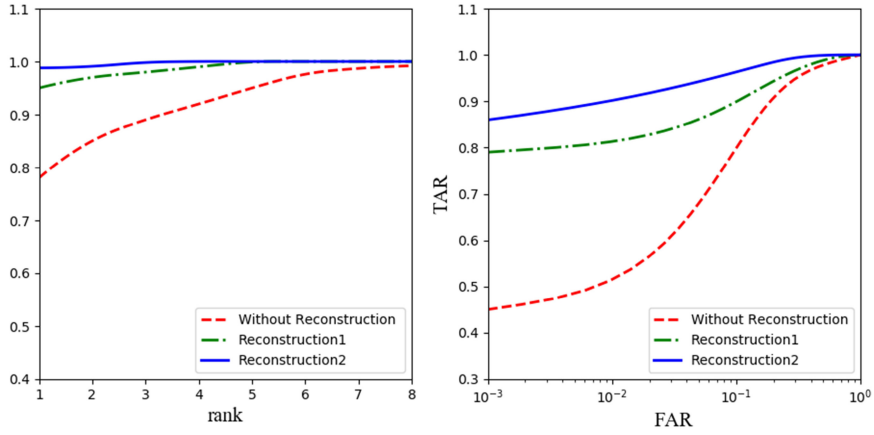

Fig. 11. The CMC and ROC results of three methods in FRGC2.0.

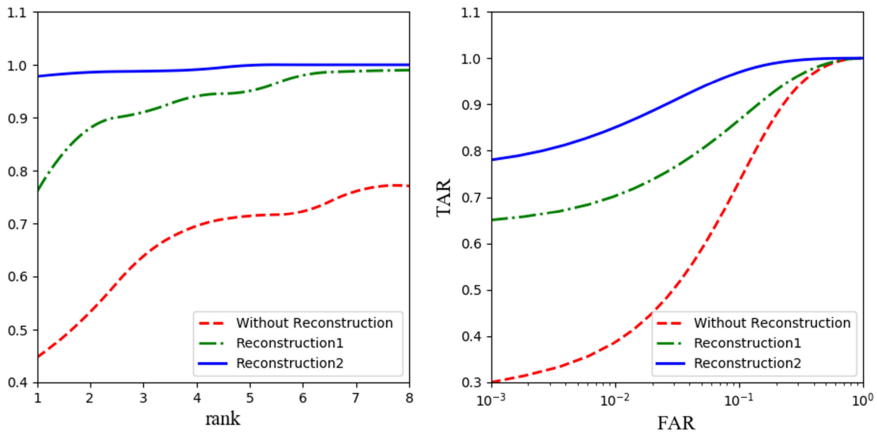

Fig. 12. The CMC and ROC results of two methods in BosphorusDB.

surface region analysis are used as comparison. Drira [18] extracts geodesic curves from the nasal region, but the drawback of this method has been discussed. Berretti [7] proposed a keypoints-based 3D face recognition method that represents a new trend for practical face analysis. The corresponding keypoints are detected on the facial surface and used to build the facial measurement. However, the method is not robust to rigid transfer and sensitive to the quality of the facial surface. In Table 3, we evaluate the identification rate in Rank1 of the various methods in different subsets.

8.3 Evaluation of Facial Data Organization

The facial organization improves the speed of face searching in a large facial database. The searching path can be obtained based on the structure by comparing the source FFLM to the mean FFLMs from different levels. Thus, the computational requirements of the face-searching process in a large facial database can be reduced. Drira [18] proposed a similar facial data organization by nasal geodesic curves' measurement. In Table 4, we show the time cost for different methods in FRGC2.0 and BosphorusDB. As a comparison, our facial organization is better than Drira [18]. The reason is the FFLM similarity measurement is faster than curves' elastic measures.

Table 1. Identification and Verification in FRGC2.0 & BosphorusDB by Different Methods

Database	FRGC2.0		BosphorusDB	
Method	**Rank1**	**FAR0.1**	**Rank1**	**FAR0.1**
Berretti 2010	0.923	0.891	0.842	0.863
Berretti 2014	0.962	0.971	0.945	0.953
Drira 2009	0.732	0.762	0.681	0.722
Drira 2013	0.977	0.971	0.923	0.912
Li 2014	0.963	–	0.966	–
Gilani 2016	0.971	0.968	0.963	–
Ouamane 2017	–	0.968	–	0.989
Emambakhsh 2017	0.969	0.935	0.953	–
Lv 2018	–	–	0.90	0.91
Soltanpour 2019	0.993	–	0.948	–
Hawraa 2019	0.964	–	–	–
Our Method	0.981	0.985	0.971	0.973

Table 2. Identification Rate of Rank1 in Different Subsets of BosphorusDB

Method	Neutral vs. Expressions	Neutral vs. Neutral	Neutral vs. All
Berretti 2010	0.896	0.923	0.812
Berretti 2014	0.915	0.979	0.934
Drira 2009	0.653	0.814	0.796
Drira 2013	0.956	0.982	0.956
Li 2014	0.961	0.972	0.952
Gilani 2016	0.967	–	0.979
Ouamane 2017	–	–	0.9617
Emambakhsh 2017	–	–	0.953
Soltanpour 2019	0.977	–	0.948
Our Method	0.968	0.988	0.979

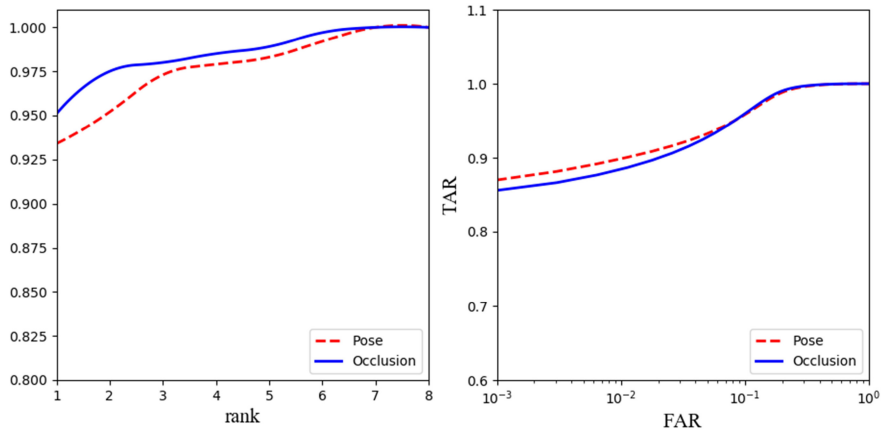

Fig. 13. The CMC and ROC results of our method in different subsets of BosphorusDB.

Table 3. Identification Rate of Rank1 in Different Subsets of BosphorusDB (Poses and Occlusions)

Method	Pose [−45,+45]	Occlusions (hand, hair, and glasses)
Berretti 2010	0.552	0.652
Berretti 2014	0.915	0.932
Drira 2009	0.721	0.743
Drira 2013	–	0.87
Li 2014	0.911	0.992
Gilani 2016	0.882	0.973
Lv 2018	0.91	0.87
Our Method	0.934	0.951

Table 4. The Comparison of Speed Searching by Different Facial Recognition Methods

Database	FRGC2.0		BosphorusDB	
Method	**Average time**	**Average time in structure**	**Average time**	**Average time in structure**
Drira 2009	183 s	27 s	110 s	27 s
Berriti 2010	47 s	–	38s	–
Gilani 2016	>300s	–	>300s	–
Ouamane 2017	>300s	–	>300s	–
Our Method	65 s	17 s	43 s	11 s

9 CONCLUSION

We present a novel 3D facial similarity measurement based on Kendall shape space theory. The advantages of our measurement are robustness to similarity transformation, facial expressions, and different types of occlusions. The experimental results show that our framework can achieve accurate facial similarity measures results and improve the speed of the face searching. In future work, we will focus on reducing the complexity of the facial landmarks and additional keypoints extraction algorithm. We also plan to improve the accuracy of the partial facial data registration and the efficiency of the face cropping in raw facial data.

ACKNOWLEDGMENTS

We would like to thank the code providers (Geodesiclib: http://www.cs.technion.ac.il/~vitus/geolib.html; NonrigidICP: https://github.com/charlienash/nricp; 3D facial landmarks detection: http://www.cipa.dcu.ie/code.html) and data providers (Kun Zhou for Facewarehouse, Sankur for BosphorusDB, and Flynn for FRGC2.0). We would also like to thank the hardware support (TITAN XP) from NVIDIA.

REFERENCES

[1] R. Ahdid, S. Safi, M. Fakir, and B. Manaut.2017. Geodesic distance on Riemannian manifold using Jacobi iterations in 3D face recognition system. *Int. J. Inf. Commun. Technol.* 6, 1 (2017), 10–19.

[2] R. Ahdid, S. Safi, and B. Manaut. 2015. Three dimensional face surfaces analysis using geodesic distance. *J. Comput. Sci. Applic.* 3 (2015), 67–72.

[3] B. Amberg, S. Romdhani, and T. Vetter. 2007. Optimal step nonrigid ICP algorithms for surface registration. In *IEEE Conference on Computer Vision and Pattern Recognition (CVPR'07)*. 1–8.
[4] A. N. Ansari and M. Abdel-Mottaleb. 2005. Automatic facial feature extraction and 3D face modeling using two orthogonal views with application to 3D face recognition. *Pattern Recog.* 38, 12 (2005), 2549–2563.
[5] S. Berretti, A. Bimbo, and P. Pala. 2010. 3D face recognition using iso-geodesic stripes. *IEEE Trans. Pattern Anal. Mach. Intell.* 32, 12 (2010), 2162–2177.
[6] S. Berretti, N. Werghi, A. D. Bimbo et al. 2013. Matching 3D face scans using interest points and local histogram descriptors. *Comput. Graph.* 37, 5 (2013), 509–525.
[7] S. Berretti, N. Werghi, A. D. Bimbo, et al. 2014. Selecting stable key points and local descriptors for person identification using 3D face scans. *Vis. Comput.* 30, 11 (2014), 1275–1292.
[8] V. Blanz and T. Vetter. 2003. Shape analysis of elastic curves in Euclidean spaces. *IEEE Trans. Pattern Anal. Mach. Intell.* 25, 9 (2003), 1063–1074.
[9] J. Booth, A. Roussos, A. Ponniah, et al. 2018. Large scale 3D morphable models. *Int. J. Comput. Vis.* 126, 2–4 (2018), 233–254.
[10] A. M. Bronstein, M. M. Bronstein, R. Kimmel, et al. 2005. Three dimensional face recognition. *Int. J. Comput. Vis.* 64, 1 (2005), 5–30.
[11] C. Cao, Y. Weng, K. Zhou, et al. 2014. FaceWarehouse: A 3D facial expression database for visual computing. *IEEE Trans. Vis. Comput. Graph.* 20, 3 (2014), 413–425.
[12] H. Chen and B. Bhanu. 2007. Human ear recognition in 3D. *IEEE Trans. Pattern Anal. Mach. Intell.* 29, 4 (2007), 718–737.
[13] T. F. Cootes, G. J. Edwards, and C. J. Taylor. 2001. Active appearance models. *IEEE Trans. Pattern Anal. Mach. Intell.* 23, 6 (2001), 681–685.
[14] T. F. Cootes, C. J. Taylor, D. H. Cooper, and J. Graham. 1995. Active shape models—their training and application. *Comput. Vis. Image Underst.* 61, 1 (1995), 38–59.
[15] C. Ding and D. Tao. 2015. Robust face recognition via multimodal deep face representation. *IEEE Trans. Multimedia* 17, 11 (2015), 2049–2058.
[16] C. Dorai and A. K. Jain. 1997. COSMOS-A representation scheme for 3D free-form objects. *IEEE Trans. Pattern Anal. Mach. Intell.* 19, 10 (1997), 1115–1130.
[17] H. Drira, B. B. Amor, A. Srivastava, et al. 2013. 3D face recognition under expressions, occlusions, and pose variations. *IEEE Trans. Pattern Anal. Mach. Intell.* 35, 9 (2013), 2270–2283.
[18] H. Drira, B. B. Amor, A. Srivastava, and M. Daoudi. 2009. A Riemannian analysis of 3D nose shapes for partial human biometrics. In *Proceedings of the IEEE International Conference on Computer Vision*. 2050–2057.
[19] I. L. Dryden, A. Kume, Le Huiling, et al. 2008. A multi-dimensional scaling approach to shape analysis. *Biometrika* 95, 4 (2008), 779–798.
[20] B. Efraty, E. Bilgazyev, S. Shah, et al. 2012. Profile-based 3D-aided face recognition. *Pattern Recog.* 45, 1 (2012), 43–53.
[21] M. Emambakhsh and A. Evans. 2016. Nasal patches and curves for expression-robust 3D face recognition. *IEEE Trans. Pattern Anal. Mach. Intell.* 39, 5 (2016), 995–1007.
[22] C. Ferrari, G. Lisanti, S. Berretti, et al. 2017. A dictionary learning based 3D morphable shape model. *IEEE Trans. Multimedia* 19, 12 (2017), 2666–2058.
[23] B. J. Frey and D. Dueck. 2007. Clustering by passing messages between data points. *Science* 315, 5814 (2007), 972–976.
[24] A. V. Gaikwad, S. J. Shigwan, and S. P. Awate. 2015. A statistical model for smooth shapes in Kendall shape space. In *Medical Image Computing and Computer-Assisted Intervention (MICCAI'15)*, N. Navab, J. Hornegger, W. Wells, and A. Frangi (Eds.), Vol. 9351. 628–635.
[25] S. Ganguly, D. Bhattacharjee, and M. Nasipuri. 2017. Fuzzy matching of edge and curvature based features from range images for 3D face recognition. *Intell. Autom. Soft Comput.* 23, 1 (2017), 51–62.
[26] S. Z. Gilani and A. Mian. 2016. Towards large-scale 3D face recognition. In *Proceedings of the IEEE International Conference on Digital Image Computing: Techniques and Applications*. 1–8.
[27] S. Gilani, A. Mian, and P. Eastwood. 2017. Deep, dense and accurate 3D face correspondence for generating population specific deformable models. *Pattern Recog.* 69 (2017), 238–250.
[28] S. Z. Gilani, F. Shafait, and A. Mian. 2015. Shape-based automatic detection of a large number of 3D facial landmarks. In *Proceedings of the IEEE Conference on Computer Vision and Pattern Recognition*. 4639–4648.
[29] B. Gokberk, A. Ali Salah, and L. Akarun. 2005. Rank-based decision fusion for 3D shape-based face recognition. *Audio Video-based Biomet. Person Authent.* 3246 (2005), 1019–1028.
[30] H. Hawraa, Z. Bilal, and K. Ahmed. 2019. 3D face factorisation for face recognition using pattern recognition algorithms. *Cyber. Inf. Technol.* 19, 2 (2019), 28–37.
[31] D. Huang, M. Ardabilian, Y. Wang, et al. 2012. 3-D face recognition using eLBP-based facial description and local feature hybrid matching. *IEEE Trans. Inf. Forens. Sec.* 7, 5 (2012), 1551–1565.

[32] S. Jahanbin, H. Choi, Y. Liu, et al. 2008. Three dimensional face recognition using iso-geodesic and iso-depth curves. In *Proceedings of the IEEE International Conference on Biometrics: Theory, Applications and Systems*. 1–6.
[33] S. Jahanbin, R. Jahanbin, A. C. Bovik, et al. 2013. Passive three dimensional face recognition using iso-geodesic contours and procrustes analysis. *Int. J. Comput. Vis.* 105, 1 (2013), 87–108.
[34] A. E. Johnson. 1997. *Spin Images: A Representation for 3-D Surface Matching*. Ph.D. Dissertation. Carnegie Mellon University, Pittsburgh, PA.
[35] M. Kafai, K. Eshghi, and B. Bhanu. 2014. Discrete cosine transform locality-sensitive hashes for face retrieval. *IEEE Trans. Multimedia* 16, 4 (2014), 1090–1103.
[36] D. G. Kendall. 1984. Shape manifolds, procrustean metrics, and complex projective spaces. *Bull. London Math. Soc.* 16, 2 (1984), 81–121.
[37] P. Koppen, Z. Feng, J. Kittler, et al. 2018. Gaussian mixture 3D morphable face model. *Pattern Recog.* 74 (2018), 617–628.
[38] S. Kurtek and H. Drira. 2015. A comprehensive statistical framework for elastic shape analysis of 3D faces. *Comput. Graph.* 51 (2015), 52–59.
[39] Y. Lei, M. Bennamoun, M. Hayat, et al. 2014. An efficient 3D face recognition approach using local geometrical signatures. *Pattern Recog.* 47, 2 (2014), 509–524.
[40] H. Li, D. Huang, J. M. Morvan, et al. 2015. Towards 3D face recognition in the real: A registration-free approach using fine-grained matching of 3D keypoint descriptors. *Int. J. Comput. Vis.* 113, 2 (2015), 128–142.
[41] H. Li, J. Sun, Z. Xu, et al. 2017. Multimodal 2D+3D facial expression recognition with deep fusion convolutional neural network. *IEEE Trans. Multimedia* 19, 12 (2017), 2816–2831.
[42] C. Lv, Z. Wu, X. Wang, and M. Zhou. 2019. 3D facial expression modeling based on facial landmarks in single image. *Neurocomputing* 355 (2019), 155–162.
[43] C. Lv, Z. Wu, X. Wang, M. Zhou, and K. Toh. 2019. Nasal similarity measure of 3D faces based on curve shape space. *Pattern Recog.* 88 (2019), 458–469.
[44] C. Lv and J. Zhao. 2018. 3D face recognition based on local conformal parameterization and iso-geodesic stripes analysis. *Math. Prob. Eng.* 2018 (2018), 1–10.
[45] Z. Wang, M. Xu, Y. Ren, et al. 2018. Saliency detection in face videos: A data-driven approach. *IEEE Trans. Multimedia* 20, 6 (2018), 1335–1349.
[46] S. A. Mahmood, R. F. Ghani, and A. A. Kerim. 2014. 3D face recognition using pose invariant nose region detector. In *Proceedings of the Computer Science and Electronic Engineering Conference*. 103–108.
[47] I. Mpiperis, S. Malassiotis, and M. G. Strintzis. 2008. Bilinear models for 3-D face and facial expression recognition. *IEEE Trans. Inf. Forens. Sec.* 3, 3 (2008), 498–511.
[48] A. Ouamane, A. Chouchane, et al. 2017. Efficient tensor-based 2D+3D face verification. *IEEE Trans. Inf. Forens. Sec.* 12, 11 (2017), 2751–2762.
[49] A. Patel and W. A. P. Smith. 2015. Manifold-based constraints for operations in face space. *Pattern Recog.* 52 (2015), 206–217.
[50] A. P. Pentland. 1991. Face recognition using eigenfaces. In *Proceedings of the IEEE Computer Society Conference on Computer Vision and Pattern Recognition*. 586–591.
[51] P. Perakis, G. Passalis, T. Theoharis, and I. Kakadiaris. 2013. 3D facial landmark detection under large yaw and expression variations. *IEEE Trans. Pattern Anal. Mach. Intell.* 35, 7 (2013), 1552–1564.
[52] P. J. Phillips, P. J. Flynn, T. Scruggs, et al. 2006. Preliminary face recognition grand challenge results. *Autom. Face Gest. Recog.* 15–24.
[53] A. Savran, N. Alyuz, H. Dibeklioglu, et al. 2008. Bosphorus database for 3D face analysis. In *Proceedings of the 1st COST 2101 Workshop on Biometrics and Identity Management*. 47–56.
[54] S. Schwab, T. Chateau, C. Blanc, and L. Trassoudaine. 2013. A multi-cue spatio-temporal framework for automatic frontal face clustering in video sequences. *Eurasip J. Image Vid. Proc.* 2013, 1 (Jan. 2013), 1–12.
[55] D. Smeets, J. Keustermans, D. Vandermeulen, et al. 2013. MeshSIFT: Local surface features for 3D face recognition under expression variations and partial data. *Comput. Vis. Image Underst.* 117, 2 (2013), 158–169.
[56] S. Soltanpour and Q. Wu. 2019. Weighted extreme sparse classifier and local derivative pattern for 3D face recognition. *IEEE Trans. Image Proc.* 28, 6 (2019), 3020–3033.
[57] F. M. Sukno, J. L. Waddington, and P. F. Whelan. 2015. 3-D facial landmark localization with asymmetry patterns and shape regression from incomplete local features. *IEEE Trans. Cyber.* 45, 9 (2015), 1717–1730.
[58] V. Surazhsky, T. Surazhsky, D. Kirsanov, et al. 2005. Fast exact and approximate geodesics on meshes. *ACM Trans. Graph.* 24, 3 (2005), 553–560.
[59] Y. Tang, H. Li, X. Sun, et al. 2017. Principal curvature measures estimation and application to 3D face recognition. *J. Math. Imag. Vis.* 2017, 3 (2017), 1–23.
[60] Y. Wang, G. Pan, Z. Wu, and Y. Wang. 2006. Exploring facial expression effects in 3D face recognition using partial ICP. In *Proceedings of the Asian Conference on Computer Vision*. 3851 (2006), 581–590.

[61] P. Yan and K. W. Bowyer. 2007. Biometric recognition using 3D ear shape. *IEEE Trans. Pattern Anal. Mach. Intell.* 29, 8 (2007), 1297–1308.
[62] L. Yuan, W. Liu, and Y. Li. 2016. Non-negative dictionary based sparse representation classification for ear recognition with occlusion. *Neurocomputing* 171, C (2016), 540–550.
[63] W. Zeng, D. Samaras, and X. Gu. 2010. Ricci flow for 3D shape analysis. *IEEE Trans. Pattern Anal. Mach. Intell.* 32, 4 (2010), 662–677.
[64] L. Zhang, L. Li, H. Li, et al. 2016. 3D ear identification using block-wise statistics-based features and LC-KSVD. *IEEE Trans. Multimedia* 18, 8 (2016), 1531–1541.
[65] X. Zhu, Z. Lei, J. Yan, et al. 2015. High-fidelity pose and expression normalization for face recognition in the wild. *Comput. Vis. Pattern Recog.* 787–796.

Received November 2019; revised April 2020; accepted April 2020